Applied Thermal Engineering 61 (2013) 355–363

Contents lists available at ScienceDirect

Applied Thermal Engineering

journal homepage: www.elsevier.com/locate/apthermeng

Waste heat recovery from a diesel engine using shell and tube heat exchanger

Saiful Bari*, Shekh N. Hossain

Barbara Hardy Institute, School of Engineering, University of South Australia, Mawson Lakes Campus, SA 5095, Australia

HIGHLIGHTS

- Diesel engine exhaust contains 38% energy which can be used to produce extra power.
- Optimum pressure of fluid exists for maximum power which was 30 bar for this study.
- The optimum pressure at 25%, 83%, 100% loads were 2, 20 and 30 bar, respectively.
- Extra 24% power gained with optimized heat exchangers using water as working fluid.
- Parallel heat exchangers showed better performance than series up to 30 bar.

ARTICLE INFO

Article history:
Received 17 March 2013
Accepted 14 August 2013
Available online 26 August 2013

Keywords:
Exhaust heat recovery
Diesel engine
Rankine Cycle
Heat exchanger

ABSTRACT

Exhaust heat from diesel engines can be an important heat source to provide additional power using a separate Rankine Cycle. In this study, experiments were conducted using water as the working fluid to estimate the exhaust waste heat obtainable from a diesel engine using two available heat exchangers purchased from the marketplace. An additional power of 16% was found. As these heat exchangers were not specifically designed for this application, attempts were then made to improve the overall performance of the exhaust heat recovery system by optimizing the design of the heat exchangers. The working fluid pressure and the orientation of heat exchangers were also optimized. After optimization, the additional power increased from 16% to 23.7%.

1. Introduction

Today's modern life heavily relies on Internal Combustion Engines (ICEs). Despite the fact that some new technologies have been introduced in recent years, the majority of vehicles are still powered by either Spark Ignition (SI) or Compression Ignition (CI) engines. CI engines, also known as diesel engines, possess a wide field of applications as energy converters because of their higher efficiency. Governments and diesel engine manufacturers are motivated to mitigate emissions and improve fuel efficiency of diesel engines due to rising greenhouse gas emissions, fossil fuel depletion and increasing fuel costs. Consequently, various efforts have been made in recent years to further improve diesel engine efficiency. Direct Injection (DI) technology, Homogeneous Charge Compression Ignition (HCCI) technology [1,2], combination of advanced injection timing, high injection pressure, and high boost pressure [3] have been developed to improve the performance of engines. Higher diesel engine efficiency can also be attained by improving thermodynamic efficiency of the operating cycle or by reducing mechanical losses [4].

Regardless of the improvements in efficiency, diesel engines continue to discharge a significant portion of chemical energy of fuel in terms of heat energy to the environment through exhaust gas, coolant, lubricating oil and friction. Generally at full load, a typical diesel engine can convert around 38% [5] of its input energy to useful work whereas 30% is wasted through the engine exhaust gas, 25% through the coolant and lubricating oil and the remaining 7% to the frictional losses [6–9]. Due to the presence of 30% waste heat in the exhaust gas, a typical heavy duty diesel engine exhaust temperature ranges from 500 to 750 °C [10] which varies with size, speed and load of the engine. The exhaust gas has higher recovery potential than the coolant because of higher temperature and exergy [11]. This high exhaust temperature provides a significant opportunity to recover heat using exhaust heat recovery (EHR) technology for various applications. This can contribute to a substantial improvement to the overall efficiency of a diesel engine [12].

* Corresponding author. Tel.: +61 8 8302 3439; fax: +61 8 8302 3380.
E-mail address: saiful.bari@unisa.edu.au (S. Bari).

1359-4311/$ – see front matter © 2013 Elsevier Ltd. All rights reserved.
http://dx.doi.org/10.1016/j.applthermaleng.2013.08.020

Turbocharging, cabin air-heating [13], desalination [14] and reducing engine warm-up time [15] are conventional technologies to utilize EHR, but with a low recovery rate. Relatively new major technologies of EHR including turbo-compounding and thermal EHR are based on the Rankine Cycle (RC) and Thermoelectric (TE) regenerations. In RC based EHR, a steam generator is employed to generate steam from the exhaust heat which is expanded in a steam turbine to produce additional power. In a turbo-compounding system, an additional power turbine is utilized downstream of the turbocharger. Here it is mechanically coupled to the engine crank shaft by a gear train to increase the engine power output [16]. However, increase in the engine backpressure and pumping loss [17] are fatal disadvantages of a turbo-compounding system. Consequently, the turbo-compounding system is not widely utilized. Dolze et al. [18] performed a thermodynamic analysis to investigate the EHR from stationary engines. They reported an 8.5% improvement in the thermal efficiency of the EHR using a RC system from the exhaust of the engine. The outstanding heat storage ability of the steam reservoir that acted as an energy buffer was emphasized to favour the RC against the turbo-compounding system. Between the RC system and the turbo-compounding of the EHR, Weerasinghe et al. [19] made a numerical simulation comparing the power output and fuel savings. The result demonstrated the relative advantage of the RC over turbo-compounding. According to their study, 7.8% of power was recovered by using the RC system whereas only 4.1% of power was recovered by using turbo-compounding. Thermoelectric generator is a sophisticated EHR technique. This technology directly converts a proportion of the exhaust gas heat to electric power through the thermoelectric phenomenon without the utilization of mechanical components [16]. Due to the low conversion efficiency of the current technology and the relatively high costs of the thermoelectric semiconductor materials, the TE is not yet suitable for practical applications [20].

A systematic approach towards using an installation based on the RC to recover heat from the exhaust of a heavy duty diesel engine dates back to the early 1970s, where a research program funded by the US Department of Energy (DOE) was conducted by Mack Trucks and Thermo Electron Corporation [21–23]. Governed by this program, an Organic Rankine Cycle (ORC) system was installed on a Mack Truck diesel engine and the lab test results revealed an improvement of the break specific fuel consumption (bsfc) of 10–12% and the result was verified by highway tests. During the following years, similar research programs were performed by other research institutes and vehicle manufacturers. Aly [24] was able to produce 16% additional power from the exhaust of a Mercedes-Benz OM422A diesel engine using ORC with R-12 as the working fluid. Srinivasan et al. [25] was able to improve the fuel conversion efficiency of about 7% on average by using ORC turbo-compounding. Koebbman [26] examined ORC systems with capacities from 750 to 1500 kWe. Recently, the utility of the RC systems have additionally increased its potential competitiveness in the market [27,28]. This is a result of technical advancements in a series of critical components for the operation of such an installation (heat exchanger, condenser and expander) but also stems from highly increased fuel prices. Nowadays, the installation of the RC to produce additional power is not only considered as a feasible solution for efficiency improvement in heavy duty diesel engines of trucks and buses [29,30], but also for light duty applications such as passenger cars [31].

With the exception of turbo-compounding, RC- and ORC-based heat recovery systems need to utilize heat exchangers to extract energy from the exhaust gas. The heat exchanger design is critical as it needs to provide an adequate surface area in order to cope with the thermal duty while adhering to the specifications of small-size and lightweight arrangements to be retrofitted in an existing vehicle. Pressure loss across the heat exchangers also needs to be reasonable to avoid back pressure that will have a negative impact on the net engine power and efficiency. However, studies of the design of the heat exchanger of EHR systems using the RC together with pressure of the working fluid, which is another important design parameter, are scarce. Furthermore, most of the work done by the researchers mentioned above is on diesel engines at full load. Engines however, can be operated at full load as well as at part loads. Therefore, this also needs to be investigated.

In this research, experiments were conducted to measure the exhaust heat available from an automotive diesel engine. Two identical shell and tube heat exchangers were purchased and installed into the engine exhaust system which was then used to produce super-heated steam. Although a turbine was not installed for this experiment, the available data sufficed to estimate the additional power using the actual turbine efficiency [32,33]. The heat exchangers used in the experiment may have not performed optimally for this particular application as they were purchased from the marketplace. Hence, research was conducted to design heat exchangers to operate optimally for this particular EHR application using commercial CFD software ANSYS CFX 14.0. The existing heat exchangers were initially modelled to validate the simulation results with the experimental results. Different parameters such as shell diameter, length, number and diameter of tubes were varied to design the optimum heat exchangers. The pressure of the working fluid and the orientation of the heat exchangers were also varied to find the optimum pressure and the best orientation. Finally, the maximum additional power achievable by these heat exchangers was estimated, thereby justifying the use of the EHR to produce additional power using the RC. This was done at the rated load of the engine; however, the performance of the EHR system was also investigated at part loads.

2. Experimental setup

The engine used in this study was a 4-stroke, 4-cylinders, water cooled Toyota 13B diesel engine. The specification of the engine is presented in Table 1. The engine was coupled with a hydraulic dynamometer. The schematic diagram of the experimental setup is shown in Fig. 1.

A nozzle was mounted at the air inlet of the engine to measure the air-flow rate. The pressure difference across the nozzle was measured with an accuracy of ±0.01 kPa using an inclined manometer. For the fuel flow measurement, a digital weighing scale with an accuracy of ±1 g and a stop watch were used. From the measured air and fuel mass flow rates, exhaust mass flow rate was calculated. Thermocouples of K type were used to measure the temperatures at different points with an accuracy of ±1 °C. Burdon tube pressure gauges were used to measure the cold and hot fluid side pressures of the heat exchangers with an accuracy of ±2%. A Dwyer model VFA variable area flow meter was used to measure the water flow rate into the heat exchangers. The flow meter had an accuracy of ±5%. Engine speed was measured by a digital tachometer with an accuracy of ±1 rpm. The heat exchangers and the exhaust piping systems were well insulated to prevent heat

Table 1
Engine specifications.

Engine model make	13B Toyota
Type of engine	4 Cylinder water cooled diesel engine
Bore	102 mm
Stroke	105 mm
Compression ratio	17.6:1
Torque	217 N m @ 2200 rpm
Injection and intake mode	Direct injection, naturally aspirated

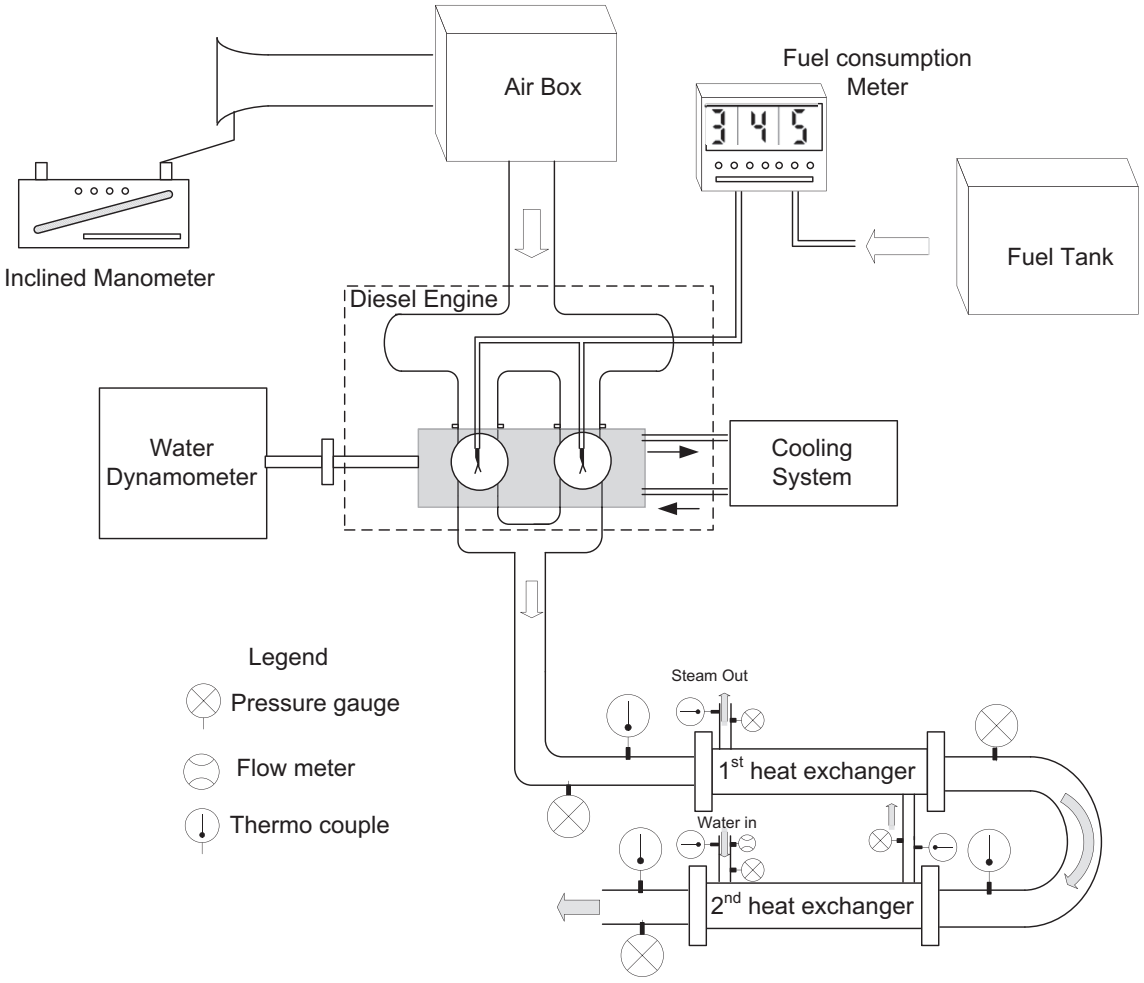

Fig. 1. Schematic diagram of the experimental setup.

losses to the ambient environment. Glass wool fibre with reflective aluminium foil was used to insulate the exhaust system and the heat exchangers. The thickness of the insulation was 60 mm and the thermal conductivity of the insulation was 0.038 W/m °C.

The engine was tested at different loads and speeds. Exhaust temperatures, fuel and air-flow rates were recorded to calculate the available heat energy from the exhaust. The exhaust of the engine was then connected to two shell and tube heat exchangers in parallel and series configurations to study the performance of the heat exchangers. Water mass flow rates, water temperatures and pressures were recorded to calculate the effectiveness of the heat exchangers. These data were used to optimize the design of the heat exchanger by computer simulations. The exhaust from the engine was passed through the tubes of the heat exchangers and the water flowed through the shell side. A counter flow heat exchanger was selected for this study. The previous work of the authors [34] suggests that the counter flow heat exchanger is more effective for the EHR system than a parallel flow heat exchanger. The additional advantages of counter flow orientation over parallel flow orientation are lower surface area requirements for the same amount of heat flow and the cold fluid exit temperature can be higher than that of the hot fluid exit temperature [35,36].

3. Heat exchanger design

Two identical shell and tube heat exchangers with a shell diameter of 76 mm, 7 tubes with diameters of 20 mm and lengths of 1 m were purchased from the marketplace. They were then fitted into the exhaust of the engine and experiments were conducted to estimate the additional energy available with this setup. As these heat exchangers were not optimized for this particular application, attempts were made to design heat exchangers that would achieve maximum additional power. Simulation tools were used to simulate the current heat exchangers using the dimensions of the purchased heat exchangers and the experimental data. After acquiring adequate agreements of simulation results with the experimental results, the effects of important parameters of the heat exchanger such as length, diameter of shell, number and diameter of tubes on the performance of the heat exchangers were then investigated. The pressure of the working fluid viz. the water was varied to find out the optimum pressure for maximum additional energy. The potential additional power was then calculated using actual turbine efficiency [32,33]. Generally, as steam expands in turbines, the steam used in this application needed to be super-heated. Therefore, two heat exchangers were used: one heat exchanger was used to generate vapour from the liquid namely vapour generator and the second heat exchanger was used to generate super-heated vapour namely super heater. These two heat exchangers can be arranged into two configurations, parallel and series as shown in Fig. 2. In the case of parallel arrangement, the exhaust from the engine is split into two streams and one enters into the vapour generator whilst the other enters the super heater. However, it was found that the exhaust gas exiting the 1st heat exchanger had additional heat which could be used to heat the 2nd heat

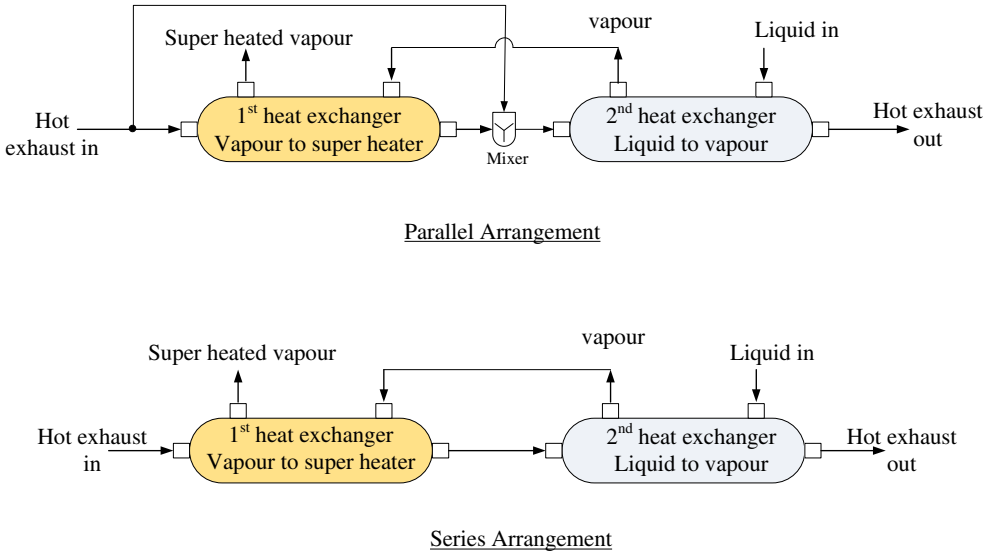

Fig. 2. Heat exchanger arrangements.

exchanger. Therefore, the exhaust gas from the 1st heat exchanger was also passed through the 2nd heat exchanger. Conversely, in series arrangement, the exhaust from the engine enters into the super heater first and then into the vapour generator as one stream. The performance of the EHR system was examined at both the parallel and series arrangements. The EHR system was designed at the rated engine power of 41.84 kW. However, the performances of the system at part loads were also examined.

4. Modelling details

4.1. Computational model

As mentioned previously, the purchased heat exchangers were modelled and simulations were carried out at first to obtain satisfactory agreements between simulation and experimental results. Then, different geometrical aspects of the heat exchanger were optimized. The existing heat exchanger model drawing was created by Computer Aided Design (CAD) software SolidWorks 2012. In the model, a 30° triangular staggered array layout was used for the tube arrangement of the heat exchanger. The geometrical model was then meshed using ANSYS meshing software. The ANSYS CFX14.0 was used to solve the equations for the fluid flow and heat transfer analysis. The CFD code ANSYS CFX is based on finite volume methods. It is a high-performance, general purpose fluid dynamics program that has been applied to solve wide-range of fluid flow and heat transfer problems.

4.2. Meshing

In order to make the simulation more accurate, different meshing schemes were used. The solid tubes were meshed using sweep mesh whereas the fluid volumes were meshed using tetragonal-hybrid elements. The final refined mesh was selected by comparing the simulation results of the model with different mesh densities and meshing schemes. Refinement of the mesh used in the computation showed some usefulness until grid independence was reached. Increasing the number of cells in the computational domain showed significant effects up to about 9,860,000 cell ranges. After this point, increasing the number of cells to around 10,760,000 showed only minor effect and then to over 12,370,000 showed no changes in the predicted cold fluid out temperature. Therefore, the final model was selected with 10,763,968 elements and 4,263,337 nodes.

4.3. Governing equations

The numerical simulation was performed with a three dimensional steady-state turbulent flow system. To solve the problem, k-ω based Shear-Stress-Transport (SST) turbulent model [37] was employed and an energy equation was included into the model. The governing equations for the flow and conjugate heat transfer were modified according to the conditions of the simulation setup. As the problem was assumed to be steady, the time dependent parameters were dropped from the equations. The resulting equations were:

$$\text{Continuity equation}: \ \nabla\cdot(\rho\vec{V}) = 0 \tag{9}$$

Momentum equations:

$$\text{x}-\text{momentum}: \ \nabla\cdot(\rho u\vec{V}) = -\frac{\partial p}{\partial x}+\frac{\partial \tau_{xx}}{\partial x}+\frac{\partial \tau_{yx}}{\partial y}+\frac{\partial \tau_{zx}}{\partial z} \tag{10}$$

$$\text{y}-\text{momentum}: \ \nabla\cdot(\rho v\vec{V}) = -\frac{\partial p}{\partial y}+\frac{\partial \tau_{xy}}{\partial x}+\frac{\partial \tau_{yy}}{\partial y}+\frac{\partial \tau_{zy}}{\partial z}+\rho g \tag{11}$$

$$\text{z}-\text{momentum}: \ \nabla\cdot(\rho w\vec{V}) = -\frac{\partial p}{\partial z}+\frac{\partial \tau_{xz}}{\partial x}+\frac{\partial \tau_{yz}}{\partial y}+\frac{\partial \tau_{zz}}{\partial z} \tag{12}$$

$$\text{Energy}: \rho c_p\left(u\frac{\partial T}{\partial x}+v\frac{\partial T}{\partial y}+w\frac{\partial T}{\partial z}\right)=\lambda\left(\frac{\partial^2 T}{\partial x^2}+\frac{\partial^2 T}{\partial y^2}+\frac{\partial^2 T}{\partial z^2}\right) \tag{13}$$

The Thermal Phase Change model [37] was used for boiling. The phase change induced by interphase heat transfer was used in this model. For this model, it was essential to consider the heat transfer processes on each side of the phase interface. Hence, the Two Resistance model [37] for interphase heat transfer was used in conjunction with the Thermal Phase Change model. Separate heat transfer processes were considered at each side of the phase interface. This was achieved by using two heat transfer coefficients

defined on each side of the phase interface designated as h_α and h_β. Then, the sensible heat flux to phase α from the interface was calculated as:

$$q_\alpha = h_\alpha(T_s - T_\alpha) \tag{14}$$

And the sensible heat flux to phase β from the interface was calculated as:

$$q_\beta = h_\beta\left(T_s - T_\beta\right) \tag{15}$$

Here, T_s is the interfacial temperature, and it was assumed to be the same for both phases. Ignoring the effects of surface tension on pressure, the interfacial temperature was assumed to be equal to the saturation temperature, T_{sat}.

The total heat flux to phase α from the interface was calculated as:

$$Q_\alpha = q_\alpha + \dot{m}_{\alpha\beta}H_{\alpha s} \tag{16}$$

and the total heat flux to phase β from the interface was calculated as:

$$Q_\beta = q_\beta - \dot{m}_{\alpha\beta}H_{\beta s} \tag{17}$$

where, $\dot{m}_{\alpha\beta}$ denotes the mass flux into phase α from phase β and $H_{\alpha s}$ & $H_{\beta s}$ represent interfacial values of enthalpy carried into and out of the phases due to the phase change.

The total heat balance $Q_\alpha + Q_\beta = 0$, then determines the interphase mass flux and is expressed as:

$$\dot{m}_{\alpha\beta} = \frac{q_{\alpha\beta} + q_{\beta\alpha}}{H_{\beta s} - H_{\alpha s}} \tag{18}$$

4.4. Boundary condition

For the heat exchanger model, water/steam was referred to as cold fluid and the exhaust gas from the engine was referred to as hot fluid. The cold fluid was considered to be in the liquid phase at 28 °C at the selected pressure and it exited as vapour from the vapour generator. It then entered into the super heater as vapour and exited as super-heated vapour at the same selected pressure. The hot fluid was modelled as air with a mass flow rate of 0.10215 kg s^{-1} and a temperature of 665 °C which were found from the experiment with the existing heat exchanger at the rated engine power of 41.84 kW. The operating pressure of hot fluid was set at 101.325 kPa and both the working pressure and mass flow rate of the cold fluid were varied.

5. Results and discussion

5.1. Experimental results

5.1.1. Exhaust temperature

In order to design an effective heat exchanger for heat recovery from the exhaust of an engine, it is essential to estimate how much energy is available in the exhaust. Therefore, some base line tests were performed without installing the heat exchangers. The exhaust gas temperatures at various speeds and powers are presented in Fig. 3. It was found from the figure that the engine power and the temperature of the exhaust gases for all three engine speeds illustrate an approximately linear relationship up to 30 kW. At powers higher than 30 kW, the exhaust temperature increases exponentially. This indicates that heat recovery will be more viable at higher powers of the engine. The maximum thermal efficiency or minimum break specific fuel consumption (bsfc) of the engine was found at 41.84 kW and 2200 rpm. The exhaust temperature at this power was found to be 665 °C and this operating point was chosen to perform the simulation to estimate the additional power obtainable with the optimized heat exchangers. However, the maximum exhaust temperature was found to be 747 °C at 45.39 kW and 2200 rpm. This point was not chosen for the design of the heat exchangers as the engine would not run continuously in this overpowered region [38–40].

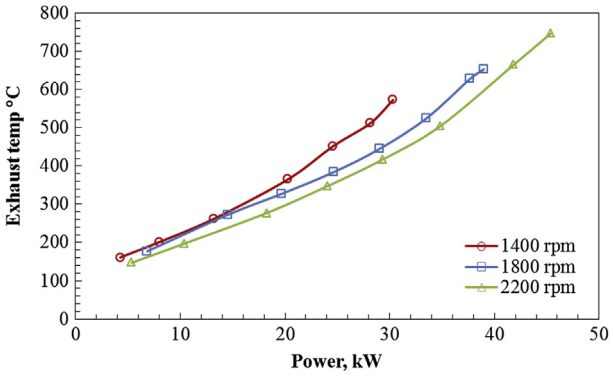

Fig. 3. Exhaust gas temperature variation with engine power.

5.1.2. Exergy calculation

Although high temperature ranges (500–750 °C) of the exhaust indicates high energy levels, only a portion of available energy can be converted into useful work [41]. Exergy analysis was carried out to determine the theoretical obtainable energy from the exhaust. Detailed exergy calculations that determine maximum obtainable energy can be found from the research works [33,42,43]. The variation of exergy with the engine power is presented in Fig. 4. It is found from the figure that up to 30 kW power, exergy has an almost linear relationship with power. At powers greater than 30 kW, the exergy increases exponentially with the power which again indicates that heat recovery is more effective at higher powers. Fig. 5 represents the effect of exhaust temperature on exergy. It is found from the graph that the exergy value of the exhaust increases with the temperature. The maximum specific exergy was found to be 437 kJ/kg at an engine speed of 2200 rpm. A similar relationship between exergy and exhaust temperature was reported in the works of Teng et al. [44]. These results indicate that approximately 50% of the engine's power is currently wasted but could be recoverable and converted to usable form. A similar conclusion was also

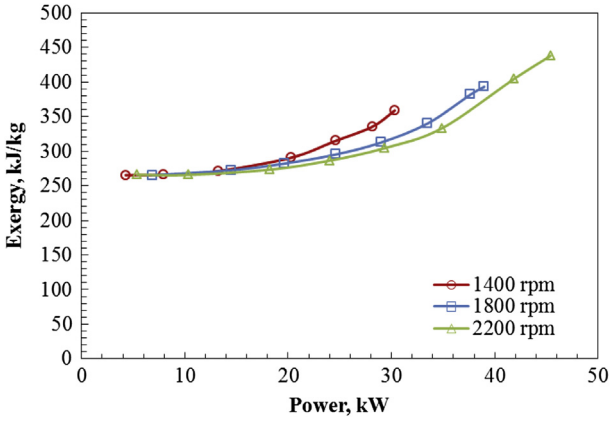

Fig. 4. Exergy variation of exhaust gas with engine power.

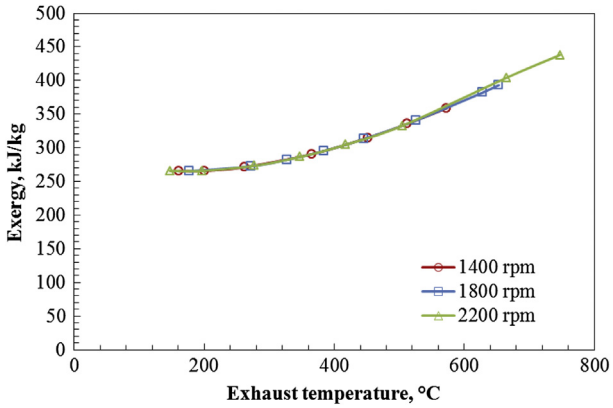

Fig. 5. Exergy variation of exhaust gas with exhaust temperature.

drawn by Hung et al. [45] and Larjola [46]. When considering heat recovery from this exhaust to produce addition power using RC, there will be some obvious losses due to friction, heat loss and irreversibility. In addition, there will be another drop of power due to heat exchanger effectiveness and turbine efficiency. Considering all these factors, there is still the possibility of increasing the engine efficiency by more than 10% [19,44,47].

5.1.3. Effectiveness of the existing heat exchanger

After the initial assessment of recoverable energy available in the exhaust of the engine, two identical shell and tube heat exchangers were installed into the exhaust system of the engine and the engine was tested at the different speeds and loads to investigate the performance of the heat exchangers. The effectiveness of the existing heat exchanger for different speeds and powers of the engine is depicted in Fig. 6. It is deduced from the figure that the maximum effectiveness of the heat exchanger occurred at an engine speed of 2200 rpm. The maximum effectiveness observed was about 0.55, which is much lower than the effectiveness reported in many literature. It is found from the literature that effectiveness can vary in the range from 0.7 to 0.99 [48,49]. Hence, there is some scope for improvement and optimization of the design of the heat exchanger to recover heat more effectively. The additional power attainable through the heat recovered by the existing heat exchangers was calculated using the actual turbine efficiency [32,33] and deducting the pump power required by the water. The maximum additional powers were found to be 6.72 kW (16.1% increase), 1.0 kW (3.0% increase) and 0.57 kW (2.0% increase) at 2200 rpm, 1800 rpm and 1400 rpm respectively. Then, the efficiency and overall efficiency of the engine with and without heat exchanger were calculated and are presented in Fig. 7. From the figure it was found that the non-optimized heat exchangers managed to improve the overall efficiency by 4.4%, 3.7% and 3.1% at maximum power at 2200 rpm, 1800 rpm and 1400 rpm, respectively. However, Teng et al. [50] achieved 15% improvement in thermal efficiency by using a binary mixture of working fluid. Therefore, it would be of interest to discover the overall efficiency improvement after the design of the heat exchanger, pressure of the working fluid and orientation of the heat exchangers are all optimized as these combinations were not done by other researchers [8,10,16–19,21,31,44,50–52].

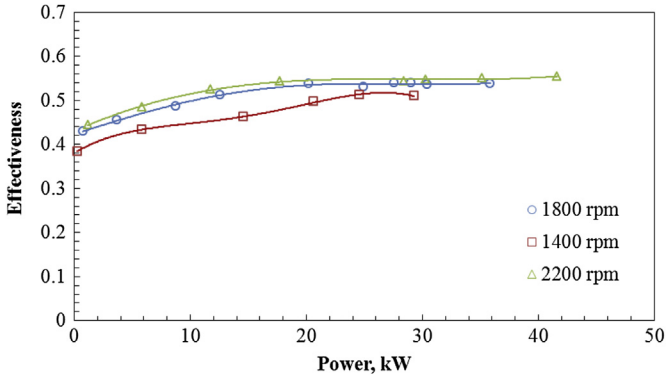

Fig. 6. Effectiveness variation with power of the existing non-optimized heat exchangers.

5.2. Model validation

The effectiveness of the existing heat exchanger found from the experimental results and CFD simulations are presented in Fig. 8. It is observed that the effectiveness predicted by CFD simulation is approximately 10% higher than the experimental values for all power ranges at 2200 rpm. The comparison was only shown for 2200 rpm as this speed was chosen to optimize the design of the heat exchangers. During the experiment, there were some sources of fouling in both the hot and the cold fluid sides. The exhaust contained soot and particles which increased resistances to the heat transfer inside the tubes and the water used in the experiment lacked treatment, consequently there were fouling on the shell as well as the tube sides. These effects were not considered in the CFD simulation. Due to these effects, the shell side and tube side heat transfer coefficients decreased [53] and thus the effectiveness reduced in the case of the experimental work. Lei et al. [54] also reported an 8% discrepancy between CFD and experimental results. Therefore, it can be concluded that the model was appropriately constructed and the experimental results and simulation results were in adequate agreement.

5.3. Heat exchanger optimization and effect of working pressure

After the validation of the model of the existing heat exchangers, the important geometrical aspects of the heat exchanger such as shell diameter & length, tube number, and number of baffles & baffle design were investigated to increase the effectiveness. As the surface area between the hot and colds fluid played an important role in heat transfer, the effect of the number of tubes on the effectiveness of the heat exchanger was examined first. The number of tubes was increased inside the initial diameter (76 mm) of the shell by reducing the tube diameter while keeping the initial diameter and length of the shell constant. It was found that the effectiveness of the heat exchanger increased as the number of tubes increased. This was due to the increase in surface area of the

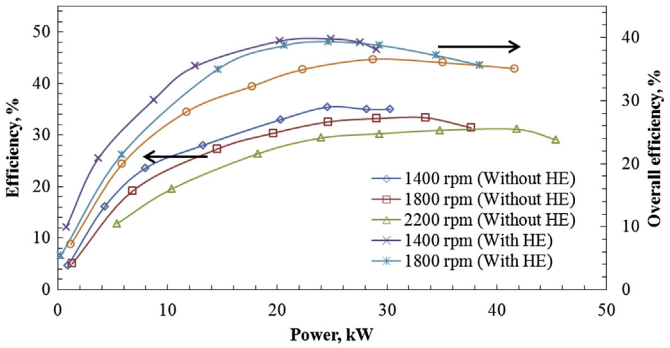

Fig. 7. Improvement of efficiency with existing heat exchangers.

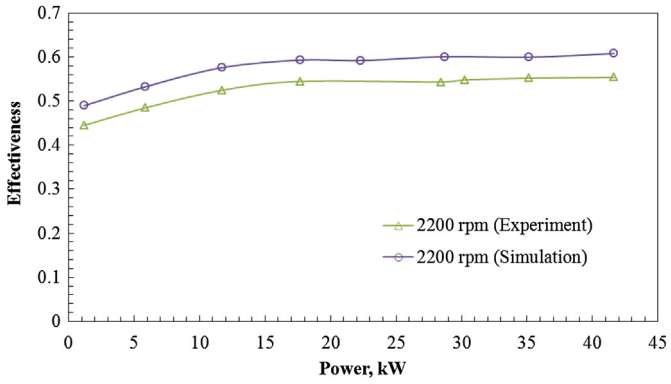

Fig. 8. Comparison of simulation and experimental results.

tubes. The additional heat transfer surfaces resulted in more heat transfer and as a result, higher effectiveness of the heat exchanger was obtained. Additionally, the shell side fluid velocity also increased with decreasing effective area of the shell side due to the increase in number of tubes. This higher velocity increased the shell side heat transfer coefficient which facilitated heat transfer [35]. Consequently, due to higher surface area and higher heat transfer, the effectiveness of the heat exchanger increased with number of tubes. Optimum number of tubes was found to be 19 for a 76 mm shell diameter.

The next important parameter that was optimized was the length of the heat exchanger. During this optimization, the number of tubes (19) and shell diameter (76 mm) were kept constant and length was increased gradually. In the case of longer heat exchanger, the hot and cold fluids received more residence time for heat transfer. As a result, the effectiveness increased with the length. Conversely, as the length increased, the heat loss to the environment also increased and the heat gain by the cold fluid could have been offset by this loss. Because of this physical phenomenon, the effectiveness of the heat exchanger increases with length up to a certain value and after this certain value, it does not increase effectively or even decreases. Similar behaviour was observed in this study. It was found that after 2 m of the length, the effectiveness slightly decreased. Therefore, the 2 m length was selected for the heat exchanger to perform further analysis.

The effect of shell diameter was investigated next after optimizing the number of tubes and the length of the heat exchangers. The diameter was varied while keeping the number of tubes (19) and length (2 m) constant. It was found that the effectiveness was higher for smaller diameter shell. As the diameter of the shell increased, the effective velocity inside the shell decreased for a fixed flow rate. The lower velocity yielded lower heat transfer coefficient [35,55] which impeded the heat transfer between the cold and hot fluids. Thus, the effectiveness was lower for a higher shell diameter. As the effectiveness decreased with increasing the diameter of the shell, the initial shell diameter of 76 mm was finally selected for the proposed heat exchanger.

After optimization, the final proposed heat exchanger had a shell diameter of 76 mm, 19 tubes, 7 baffles cut at 50%, and an effective length of 2 m. The detailed specifications of the optimized heat exchanger are presented in Table 2. The effectiveness of this heat exchanger was found to be 0.78 which is a significant improvement from the original 0.55.

The effect of different working pressure of the shell side fluid on the effectiveness of the heat exchanger was also investigated for all geometrical aspects of the heat exchanger. It was found that the effectiveness varied in insignificant quantities with pressure variations. In all cases, it was found that effectiveness was slightly

Table 2
Optimized heat exchanger specifications.

Heat exchanger type	Shell and tube counter flow, hot fluid in tubes and cold fluid in the shell
Shell inside diameter	76 mm
No of tube	19
Tube arrangement	30° triangular staggered array
Tube pitch	15 mm
Tube inside diameter	10 mm
Baffles	50% cut baffles, no. of baffle 7
Length of the heat exchanger	2 m

lower at higher pressures. At higher pressure with the same mass flow and cross-sectional area of flow, the fluid molecules are more compact. Molecular diffusion is lower and thus the heat transfer coefficient is lower. As a result, the effectiveness slightly decreased with the increasing working pressure. Thus, it can be concluded that there is negligible effect of working pressure on heat exchanger effectiveness for different parameters of the heat exchanger. Another parameter, the pressure drop across the heat exchanger should also be considered. As shown in Section 5.5, the maximum pressure drop was found to be 30.3 kPa at rated load. Due to this pressure loss the engine lost about 0.5% power which was found experimentally as shown in Fig. 7. This loss can be compensated by the additional power produced by the EHR system [40,56–58].

5.4. Additional power generation at full load

As previously mentioned, to generate additional power, two heat exchangers were used: one was a vapour generator and the other one was a super heater. From the simulation, it was found that there were no significant differences in the design of the two heat exchangers. Hence the same design was used for both heat exchangers. Extra power that could be recoverable from the exhaust of the diesel engine with the proposed shell and tube heat exchangers is presented in Fig. 9. The additional power generation was calculated at different pressures of the working fluid viz. water. The two heat exchangers could be used in two different orientations: Parallel and Series (Fig. 2). It was found that additional output power increased as the working pressure increased up to 30 bar for both the parallel and series arrangements of the heat exchangers. This is because keeping the condensing pressure constant as the working pressure increases the enthalpy drop across the turbine also increases. Interestingly however, it was found that higher power output could be achieved for parallel arrangement below 30 bar working pressure than the series arrangement, whereas series arrangement could achieve higher power output above

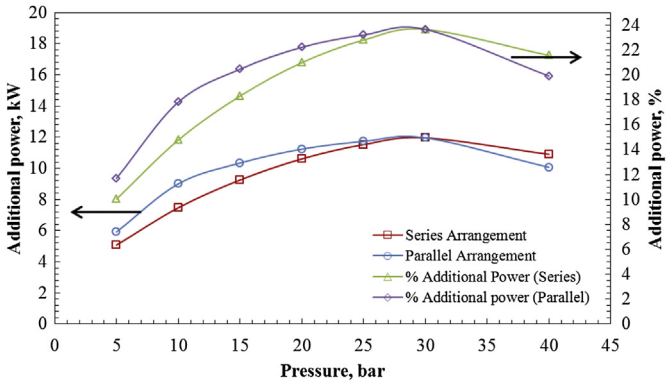

Fig. 9. Additional power output variation with working pressure.

30 bar working pressure than parallel arrangement. The enthalpy of evaporation decreases with increasing pressure. So when the parallel arrangement was used at lower pressure, more mass of steam could be generated than the series arrangement which yielded a higher additional power. The maximum power output of 9.85 kW was achieved at the 30 bar working pressure. The saturation temperature and super-heated temperature increases with pressure, so at a higher pressure, less mass of steam was generated from the same available energy of the exhaust gas. As a result the additional power generation was reduced after a certain value of the working pressure (30 bar). At 30 bar, the proposed shell and tube heat exchanger could recover 23.7% additional power from the exhaust of the diesel engine using water as the working fluid considering 70% isentropic efficiency of the turbine [32,33]. This improvement is significantly higher than those claimed by the other researchers [16–18,52] such as Aly [24] who was able to produce 16% additional power from the exhaust of a Mercedes-Benz OM422A diesel engine mounted on a 45 passengers coach. Higher achievement found in this research was due to the optimization of the design of the heat exchangers combined with the optimization of the working pressure of the fluid and orientation of the heat exchangers, which the other researchers did not perform. Due to this additional power generation the overall efficiency of the engine improved from 30% to 41%.

5.5. Additional power generation at part load

So far, the performance of the proposed EHR system with optimized design of the heat exchangers and pressure of the working fluid were investigated at the rated load of the engine. However, the automotive diesel engine can also run at part loads. Therefore, the performance of the EHR system was also evaluated at part loads of the engine. These results are presented in Fig. 10. Interestingly, it is found from the figure that after 60% load fraction, the additional power generation improves precipitously. At 25% load, the proposed system was able to produce only 3% additional power whereas at 83% load, the same system was able to generate 16% additional power and at the rated load, the EHR system was able to produce 23.7% additional power. The figure also shows the optimized pressure of the working fluid at different loads of the EHR system. It is found from the figure that the pressure needs to be changed to get the maximum power at different loads. The optimum pressures at 25%, 83% and 100% loads were 2 bar, 20 bar and 30 bar respectively. This was caused by the exhaust gas temperatures which were lower at part loads than those for higher loads. Thus, it can be concluded that the heat exchangers can recover higher power at higher load fraction of the engine. The pressure

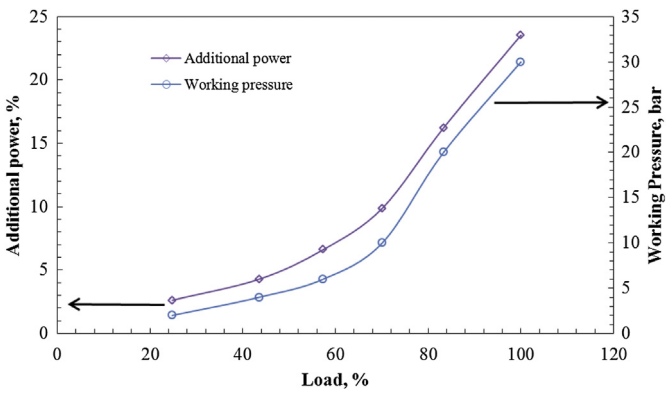

Fig. 10. Additional power and working pressure at various loads of the engine.

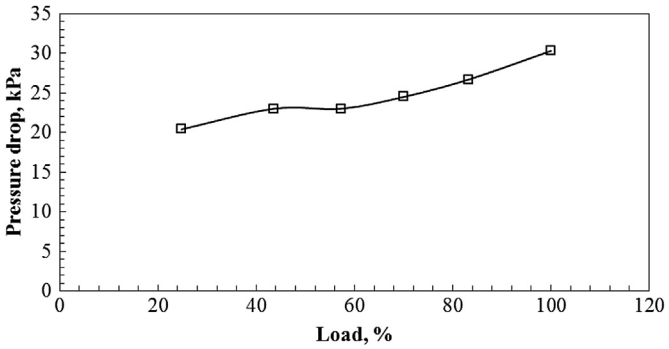

Fig. 11. Pressure drop across the heat exchanger at various loads of the engine.

drop inside the tubes through which the exhaust gas flowed need to be reasonable to avoid back pressure. Fig. 11 shows the pressure drops inside the tubes of the heat exchangers at different loads. The pressure drops varied with the load. At 25%, 83% and 100% loads, the pressure drops were 20.4, 26.7 and 30.3 kPa respectively. The engine could have lost some power due to this pressure drop. Though experiment was not conducted with the optimized heat exchangers, the experiments with the existing heat exchangers showed about 0.5% power loss as mentioned previously. Nevertheless, the additional power produced by the EHR system could compensate this loss of power.

6. Conclusions

The exhaust of a diesel engine contains about 30% of the input energy and this energy can be recovered to produce additional power using a Rankine Cycle. From the current research, the following conclusions were reached:

- There existed an optimum pressure of the working fluid for the maximum additional power conceivable by EHR system for any particular application. For this 50 kW engine, the optimum pressure was found to be 30 bar and the maximum recovered additional power was 9.85 kW.
- The design of the heat exchangers as well as their orientations was optimized for better performance of the EHR system.
- These resulted in an additional 23.7% power improvement using water as the working fluid.
- The additional power generation decreased at part loads.
- The pressure of the working fluid needed to be varied to maximize the additional power at part loads.

Acknowledgements

The authors gratefully acknowledge the financial and other support received for this project by Leartek Pty Ltd.

References

[1] Z. Şahin, O. Durgun, C. Bayram, Experimental investigation of gasoline fumigation in a single cylinder direct injection (DI) diesel engine, Energy 33 (2008) 1298–1310.
[2] K. Sudheesh, J.M. Mallikarjuna, Diethyl ether as an ignition improver for biogas homogeneous charge compression ignition (HCCI) operation – an experimental investigation, Energy 35 (2010) 3614–3622.
[3] D.T. Hountalas, G.C. Mavropoulos, T.C. Zannis, V. Schwarz, Possibilities to achieve future emission limits for HD DI diesel engines using internal measures, in: SAE Technical Paper, vol. 2005-01-0377, SAE, Detroit, MI, USA, 2005.
[4] D.T. Hountalas, T.C. Zannis, G.C. Mavropoulos, Potential benefits in heavy duty diesel engine performance and emissions from the use of variable compression ratio, in: SAE Technical Paper, Detroit, MI, USA, 2006.

[5] I. Taymaz, An experimental study of energy balance in low heat rejection diesel engine, Energy 31 (2006) 364–371.
[6] C. Yu, K.T. Chau, Thermoelectric automotive waste heat energy recovery using maximum power point tracking, Energy Convers. Manage. 50 (2009) 1506–1512.
[7] F. Stabler, Automotive applications of high efficiency thermoelectrics, in: DARPA/ONR/DOE High Efficiency Thermoelectric Workshop, 2002, pp. 1–26.
[8] E.H. Wang, H.G. Zhang, B.Y. Fan, M.G. Ouyang, Y. Zhao, Q.H. Mu, Study of working fluid selection of organic Rankine cycle (ORC) for engine waste heat recovery, Energy 36 (2011) 3406–3418.
[9] F. Yüksel, M. Ceviz, Thermal balance of a four stroke SI engine operating on hydrogen as a supplementary fuel, Energy 28 (2003) 1069–1080.
[10] T. Wang, Y. Zhang, Z. Peng, G. Shu, A review of researches on thermal exhaust heat recovery with Rankine cycle, Renewable Sustainable Energy Rev. 15 (2011) 2862–2871.
[11] M. He, X. Zhang, K. Zeng, K. Gao, A combined thermodynamic cycle used for waste heat recovery of internal combustion engine, Energy 36 (2011) 6821–6829.
[12] J. Fu, J. Liu, C. Ren, L. Wang, B. Deng, Z. Xu, An open steam power cycle used for IC engine exhaust gas energy recovery, Energy 44 (2012) 544–554.
[13] S. Jiangzhou, R.Z. Wang, Y.Z. Lu, Y.X. Xu, J.Y. Wu, Experimental study on locomotive driver cabin adsorption air conditioning prototype machine, Energy Convers. Manage. 46 (2005) 1655–1665.
[14] T.C. Hung, M.S. Shai, B.S. Pei, Cogeneration approach for near shore internal combustion power plants applied to seawater desalination, Energy Convers. Manage. 44 (2003) 1259–1273.
[15] P. Diehl, F. Haubner, S. Klopstein, F. Koch, Exhaust heat recovery system for modern cars, SAE Trans. 110 (2001) 988–998.
[16] D. Hountalas, C. Katsanos, D. Kouremenos, E. Rogdakis, Study of available exhaust gas heat recovery technologies for HD diesel engine applications, Int. J. Altern. Propul. 1 (2007) 228–249.
[17] D.T. Hountalas, C. Katsanos, V. Lamaris, Recovering Energy from the Diesel Engine Exhaust Using Mechanical and Electrical Turbocompounding, SAE Technical Paper, 2007, pp. 01–1563.
[18] V. Dolz, R. Novella, A. García, J. Sánchez, HD Diesel engine equipped with a bottoming Rankine cycle as a waste heat recovery system. Part 1: study and analysis of the waste heat energy, Appl. Therm. Eng. 36 (2012) 269–278.
[19] W.M.S.R. Weerasinghe, R.K. Stobart, S.M. Hounsham, Thermal efficiency improvement in high output diesel engines a comparison of a Rankine cycle with turbo-compounding, Appl. Therm. Eng. 30 (2010) 2253–2256.
[20] J.C. Bass, N. Elsner, F. Leavitt, Performance of the 1 KW Thermoelectric Generator for Diesel Engines, IOP (Institute Of Physics) Publishing Ltd, 1995, pp. 295–296.
[21] F. DiBella, L. DiNanno, M. Koplow, Laboratory and On-highway Testing of Diesel Organic Rankine Compound Long-haul Vehicle Engine, SAE Technical Papers, 1983.
[22] E. Doyle, L. DiNanno, S. Kramer, Installation of a Diesel-organic Rankine Compound Engine in a Class 8 Truck for a Single-vehicle Test, SAE Technical Papers, 1979.
[23] P. Patel, E.F. Doyle, Compounding the Truck Diesel Engine with an Organic Rankine-cycle System, SAE Technical Papers, 1976.
[24] S.E. Aly, Diesel engine waste-heat power cycle, Appl. Energy 29 (1988) 179–189.
[25] K.K. Srinivasan, P.J. Mago, S.R. Krishnan, Analysis of exhaust waste heat recovery from a dual fuel low temperature combustion engine using an Organic Rankine Cycle, Energy 35 (2010) 2387–2399.
[26] W. Koebbeman, Geothermal Wellhead Application of a 1-MW Industrial ORC Power System, vol. 85CH2242, IEEE, Piscataway, NJ, 1985, pp. 1387–1396.
[27] S. Hounsham, R. Stobart, A. Cooke, P. Childs, 2008-01-0309 Energy Recovery Systems for Engines, 2153, SAE SP, 2008, p. 79.
[28] M. Kadota, K. Yamamoto, Advanced transient simulation on hybrid vehicle using Rankine cycle system, SAE Int. J. Engines 1 (2009) 240.
[29] C. Nelson, Exhaust energy recovery, in: Diesel Engine-efficiency and Emissions Research (DEER) Conference, Dearborn, Michigan, 2010, pp. 242–250.
[30] R.W. Kruiswyk, An engine system approach to exhaust waste heat recovery, in: Diesel Engine-efficiency and Emissions Research (DEER) Conference, Dearborn, Michigan, 2008.
[31] J. Ringler, M. Seifert, V. Guyotot, W. Hübner, Rankine cycle for waste heat recovery of IC engines, SAE Int. J. Engines 2 (2009) 67.
[32] Y.A. Cengel, R.H. Turner, J.M. Cimbala, Fundamentals of Thermal-fluid Sciences, third ed., McGrawHill, Singapore, 2008.
[33] M.J. Moran, H.N. Shapiro, Fundamentals of Engineeering Thermodynamics, fourth ed., John Wiley & Sons, USA, 2000.
[34] S. Hossain, S. Bari, Additional Power Generation from the Exhaust Gas of Diesel Engine by Bottoming Rankine Cycle. SAE Technical Paper, 2013-01-1639, 2013.
[35] F. Kreith, R.M. Manglik, M.S. Bohn, Principles of Heat Transfer, Thomson Engineering, New York, USA, 2010.
[36] M.N. Ozisik, Heat Transfer: a Basic Approach, 1985.
[37] Ansys CFX-solver Theory Guide, Ansys Inc, 2012.
[38] A. Ibrahim, S. Bari, A comparison between EGR and lean-burn strategies employed in a natural gas SI engine using a two-zone combustion model, Energy Convers. Manage. 50 (2009) 3129–3139.
[39] A. Ibrahim, S. Bari, An experimental investigation on the use of EGR in a supercharged natural gas SI engine, Fuel 89 (2010) 1721–1730.
[40] M. Lapuerta, O. Armas, J. Rodríguez-Fernández, Effect of biodiesel fuels on diesel engine emissions, Prog. Energy Combust. Sci. 34 (2008) 198–223.
[41] J. Keenan, A system Chart for second Law analysis, ASME Mech. Eng. 54 (1932) 195–204.
[42] J.E. Ahern, Exergy Method of Energy Systems Analysis, John Wiley and Sons, New York, United States, 1980.
[43] H.D. Baehr, Thermodynamik, Springer, Germany, 2005.
[44] H. Teng, G. Regner, C. Cowland, Waste Heat Recovery of Heavy-duty Diesel Engines by Organic Rankine Cycle Part I: Hybrid Energy System of Diesel and Rankine Engines, SAE Technical Paper, 2007, pp. 01–0537.
[45] T.C. Hung, T.Y. Shai, S.K. Wang, A review of organic rankine cycles (ORCs) for the recovery of low-grade waste heat, Energy 22 (1997) 661–667.
[46] J. L., Electricity from industrial waste heat using high-speed organic Rankine cycle (ORC), Int. J. Prod. Econ. 41 (1995) 227–235.
[47] C. Leising, G. Purohit, S. DeGrey, J. Finegold, Waste heat recovery in truck engines, in: Society of Automotive Engineers, 400 Commonwealth Dr, Warrendale, PA, 15096, USA, 1978.
[48] B. Alireza, Simple method for estimation of effectiveness in one tube pass and one shell pass counter-flow heat exchangers, Appl. Energy 88 (2011) 4191–4196.
[49] J. Guo, M. Xu, L. Cheng, The application of field synergy number in shell-and-tube heat exchanger optimization design, Appl. Energy 86 (2009) 2079–2087.
[50] H. Teng, G. Regner, C. Cowland, Waste Heat Recovery of Heavy-duty Diesel Engines by Organic Rankine Cycle Part II: Working Fluids for WHR-ORC, SAE Technical Paper, 2007, pp. 01–0543.
[51] A. Domingues, H. Santos, M. Costa, Analysis of vehicle exhaust waste heat recovery potential using a Rankine cycle, Energy 49 (2013) 71–85.
[52] I. Vaja, A. Gambarotta, Internal combustion engine (ICE) bottoming with organic Rankine cycles (ORCs), Energy 35 (2010) 1084–1093.
[53] K.J. Bell, Heat Exchangers: Thermal-hydraulic Fundamentals and Design, Delaware Method for Shell Side Design, 1981, pp. 581–618.
[54] Y.G. Lei, Y.L. He, P. Chu, R. Li, Design and optimization of heat exchangers with helical baffles, Chem. Eng. Sci. 63 (2008) 4386–4395.
[55] J. Holman, Heat Transfer, eight ed., McGraw-Hill Book Company (UK) Ltd., London, England, 1997.
[56] S. Hossain, S. Bari, Effect of different working fluids on shell and tube heat exchanger to recover heat from exhaust of an automotive diesel engine, in: World Renewable Energy Congress 2011 Linköping, Sweden, 2011, pp. 764–771.
[57] S.N.H. Rubaiyat, S. Bari, Waste heat recovery using shell and tube heat exchanger from the exhaust of an automotive engine, in: 13th Asian Congress of Fluid Mechanics, Dhaka, Bangladesh, 2010, pp. 864–867.
[58] S. Bari, C. Yu, T. Lim, Filter clogging and power loss issues while running a diesel engine with waste cooking oil, Proc. Inst. Mech. Eng. Part D 216 (2002) 993–1001.

Glossary

c_p: specific heat at constant pressure, kJ/kgK
$\vec{V}$: velocity vector, m/s
u,v,w: velocity components in x, y and z direction, respectively, m/s
T: temperature, K
p: pressure, N/m^2
λ: conductivity coefficient at bulk temperature of fluid, W/m K
ρ: fluid density, kg/m^3
τ: shear stress, N/m^2
g: gravitational acceleration, m/s^2
h_α: heat transfer coefficient of α phase, W/m^{2}K
h_β: heat transfer coefficient of β phase, W/m^{2}K
q_α: sensible heat flux to α phase, W/m^2
q_β: sensible heat flux to β phase, W/m^2
T_s: interfacial temperature, K
Q: total heat flux, W/m^2
$\dot{m}_{\alpha\beta}$: mass flux from phase β to phase α
$H_{\alpha s}$, $H_{\beta s}$: interfacial values of enthalpy carried into and out of the phases due to phase change, kJ/kg